Journal of Solid State Chemistry **145,** 460–470 (1999)
Article ID jssc.1999.8154, available online at http://www.idealibrary.com on IDEAL®

Influence of the Mode of Water Coordination on the Electronic Structure of the $[V(OH_2)_6]^{3+}$ Cation

Philip L. W. Tregenna-Piggott,*,† Stephen P. Best,†,‡,[1,2] Hans U. Güdel,*,[1] Høgni Weihe,§ and Chick C. Wilson‖

*Department of Chemistry, University of Bern, Freiestrasse 3, Bern 9, CH-3000, Switzerland; †Department of Chemistry, University College London, 20 Gordon Street, London WC1H 0AJ, England; ‡School of Chemistry, University of Melbourne, Parkville, Victoria 3052, Australia; §Institute of Chemistry, Universitetsparken 5, DK-2100 Copenhagen, Denmark and ‖ISIS Facility, Rutherford Appleton Laboratory, Chilton, Oxon, OX11 0QX, England

Received September 29, 1998; in revised form December 2, 1998; accepted December 14, 1998

DEDICATED TO PETER DAY ON THE OCCASION OF HIS 60TH BIRTHDAY

The correlation between the stereochemistry and electronic structure of the $[V(OH_2)_6]^{3+}$ cation has been examined using a variety of physical techniques in conjunction with angular overlap model calculations. The experimental data includes the first reported high-field, high-frequency EPR study of a vanadium(III) complex which enables a precise determination of the ground term spin-Hamiltonian parameters. The electronic structure and vibrational spectrum of the $[V(OH_2)_6]^{3+}$ cation was studied in samples formed from the co-crystallization of $RbV(SO_4)_2 \cdot 12H_2O$ and $RbGa(SO_4)_2 \cdot 12H_2O$. The structural modifications of these salts differ in terms of the orientation of the water molecules about the tervalent cation while the $M^{III}O_6$ framework remains approximately octahedral. The electronic structure of the $[V(OH_2)_6]^{3+}$ cation in samples of Rb[Ga:V] $(SO_4)_2 \cdot 12H_2O$ is found to depend greatly on the relative proportions of gallium(III) and vanadium(III). The experimental data are in accordance with predictions based on the angular overlap model when the π-bonding normal to the plane of the water molecule is dominant over the in-plane interaction ($e_{\pi\perp} - e_{\pi\parallel}$ ca. 930 cm^{-1} for trigonal planar water coordination). The π-anisotropy results in a large trigonal field splitting of the $^3T_{1g}$ (O_h) ground term in $RbV(SO_4)_2 \cdot 12H_2O$ (1930 cm^{-1}) which diminishes almost to zero when $[V(OH_2)_6]^{3+}$ is doped into $RbGa(SO_4)_2 \cdot 12H_2O$, on account of the change in the orientation of the water molecules imposed by hydrogen bonding constraints. This work demonstrates the strong correlation between the stereochemistry and electronic structure of the $[V(OH_2)_6]^{3+}$ cation and accounts for the structural abnormalities reported for vanadium(III) salts of this type. © 1999 Academic Press

1. INTRODUCTION

The relationship between the molecular and electronic structure is central to our understanding of chemical and physical properties with the examination of systems which exhibit structural instability a focus of research spanning molecular and extended systems. In the solid state the observed molecular geometry will necessarily be a balance between that favored by the isolated molecule and the energetics of the lattice. This balance may result in an unfavorable molecular geometry in cases where the energetics of the lattice dominate over the isolated molecule. In this paper salts of vanadium(III) are characterized which differ in terms of the coordination geometry of the water ligand imposed upon the Jahn–Teller active vanadium(III) cation. These studies permit examination of the effect of the coordination geometry on the electronic structure of the tervalent cation.

The alums are a well-known series of cubic double salts of formula $M^{I}M^{III}(XO_4)_2 \cdot 12H_2O$ where M^{I} is a monovalent cation, M^{III} a tervalent cation, and X = sulfur or selenium (1–3). Tervalent hexa-aqua cations with M–O bond lengths ranging between Co (1.873 Å)[2] and In (2.112 Å)[2] may be accommodated within the structure, which features high site (S_6) and crystal (T_h) symmetries, and this contributes to the frequent use of these salts in studies of the electronic structure of tervalent aqua-ions (4–9). Three distinct alum types have been identified, the most common being the α and β modifications (1). In both cases the $M^{III}O_6$ framework is approximately octahedral with all O–M^{III}–O bond angles close to 90° (2), furthermore the metal(III)–water bond lengths are relatively insensitive to the alum type (3). A key difference between these two structural modifications is the stereochemistry of the coordinated water molecules (3). The coordination geometry of the tervalent cation is defined by the twist, tilt, and yaw angles of the single crystallographically distinct water molecule (Fig. 1). Typical values of these angles for α and β alums are respectively 0 and −20° (twist), 18 and 0° (tilt), and 1 and 1° (yaw) (3, 10–12). Clearly the differences between the tilt and twist angles are of most

[1]Authors to whom correspondence could be addressed.
[2]Present address: Department of Chemistry, University of Melbourne, Australia.

0022-4596/99 $30.00

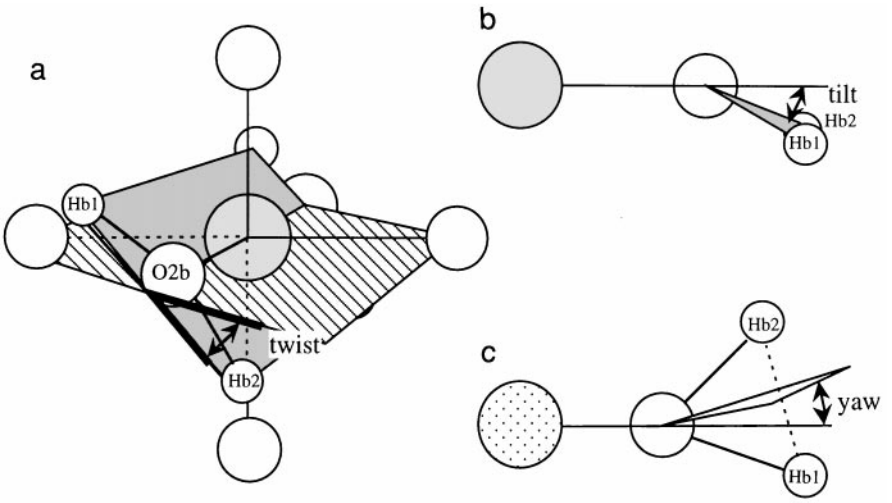

FIG. 1. Definition of the bond angles which characterise the $[M(OH_2)_6]^{3+}$ species on the S_6 sites of the alum structure. (a) Twist; this angle denotes the degree by which the H_2O plane is rotated about the M–O bond vector and is formally defined as the angle between the horizontal plane (defined with the 3-fold axis running through the top-front-right octant of the MO_6 octahedron) and the plane which contains the M–O bond vector and is parallel to the Hb1:Hb2 bond vector. For the β alums (tilt $\approx 0^\circ$) the twist angle approximates to the angle between the horizontal and the vector normal to the plane of the water molecule. The twist angle shown is $\sim -45^\circ$. (b) Tilt; angle between the M–O bond vector and the water plane. (c) Yaw; angle between the M–O bond vector and the plane normal to the water molecule which includes the oxygen atom and the point midway between the hydrogen atoms. With these definitions, the angles pertaining to the $[V(OH_2)_6]^{3+}$ cation in the $CsV(SO_4)_2 \cdot 12D_2O$ structure (32) are twist = $-$ 20.7(7)°, tilt = 0.2(7)°, and yaw = 0.9(7)°. The corresponding angles for the $[Fe(OH_2)_6]^{3+}$ cation in the $CsFe(SO_4)_2 \cdot 12D_2O$ structure (3) are twist = 0.4(2)°, tilt = 18.8(10)°, and yaw = 1.1 (2)°.

significance. Generally the alum type is determined by the identity of the monovalent cation and anion (1–3), but in cases where there is unequal occupancy of the metal t_{2g} orbitals only β alums have been observed (13–15). For the rubidium sulphate alums the α modification is observed in all known cases except when the tervalent cation is titanium(III) or vanadium(III) (13–15). This difference in structural chemistry has been related to the magnitude of the trigonal field splitting of the orbitally degenerate ground terms (13, 14). When the mode of water coordination is trigonal planar there is a significant difference between the π interactions in and normal to the plane of the water molecule (16). For a complex with S_6 symmetry the magnitude of the trigonal field splitting is then strongly dependent upon the twist angle of the coordinated ligands, with the splitting of the energies of the one-electron orbitals which comprise the t_{2g} (O_h) set greatest when the twist angle is $\pm 45^\circ$ (11, 17, 18). Based on the coordination geometries of the tervalent cation in the alum structures a much larger trigonal field splitting is expected for the β alums. In cases where there is unequal occupancy of the metal t_{2g} orbitals the trigonal field splitting provides an electronic stabilization of the β structure. For the rubidium sulfate titanium and vanadium alums the resulting electronic stabilization more than compensates for the otherwise unfavorable coordination geometry imposed on the monovalent cation. A measure of the trigonal field splitting of the $^3T_{1g}$ (O_h) ground term has been obtained indirectly, from magnetic susceptibility measurements (19) and directly from the observation of the $^3A_g \rightarrow {}^3E_g$ electronic Raman band which occurs at ca. 1940 cm^{-1} in the vanadium(III) alums of Cs^+ (20), NH_4^+ (20), Tl^+ (21), and Rb^+ (13). The structural preference of the vanadium alums is highlighted by comparison of the structures of the rubidium sulfate alums of the similarly sized cations of gallium(III) and vanadium(III) which give α and β alums, respectively (13). By doping low concentrations of vanadium(III) into the rubidium gallium sulfate alum, it is possible to alter the mode of water coordination to vanadium(III) without significantly affecting the vanadium(III)–water bond length. The electronic structure of the doped crystals has been probed by a range of physical techniques which include electronic spectroscopy, single crystal electronic and vibrational Raman spectroscopy, and EPR spectroscopy. The interpretation of these results has been assisted by ligand-field calculations.

2. EXPERIMENTAL

Synthesis

$RbV(SO_4)_2 \cdot 12H_2O$ (RbVSH) and $RbGa(SO_4)_2 \cdot 12H_2O$ (RbGaSH) were prepared by methods analogous to those of the corresponding caesium alums (22). Mixed crystals of RbVSH and RbGaSH (Rb[Ga:V]SH) were prepared by co-crystallisation of the respective alums in H_2SO_4 (1 M).

The size, quality, and alum modification of the resulting crystals were all found to depend greatly on the ratio of solute to solvent and the relative amounts of vanadium(III) and gallium(III) in solution. The alum modification of the resulting crystals could be easily identified both from the morphology (predominant [210] faces are indicative of the β modification) (15) and also the color of the crystals. The Rb[Ga:V]SH alums were either blue (β) or green (α).

Blue crystals of the β type resulted from solutions in which the gallium(III)/vanadium(III) ratio was less than 4. Large (ca. 1 cm^3) clear crystals, suitable for Raman experiments could be obtained from 0.25 weight/volume (w/v) solutions of the mixed salt in H_2SO_4 (1 M) when the solution was allowed to crystallise at room temperature. The relative amounts of vanadium(III) and gallium(III) in these β Rb[Ga:V]SH crystals, determined using inductively coupled plasma atomic emission spectroscopy (ICP-AES), corresponded to the composition of the solution from which they were obtained.

A mixed crystal of Rb[Ga:V]SH, of the β type, was also synthesized with a vanadium(III) concentration of ca. 20%. However, when the crystal was disturbed upon filtration, the color changed from blue to green on the edge and then swept across the whole crystal. After ca. 1 min the phase transformation was complete, and the formerly clear blue crystal was now green and opaque. It is likely that a β to α structural change occurs, with the difference in packing efficiency resulting in a destructive phase transition. These observations suggest that the β structure is thermodynamically favored when there is, on average, more than one vanadium(III) cation per unit cell.

With a gallium(III)/vanadium(III) ratio in solution greater than ca. 5, green crystals, with predominant [111] faces, of the α type were formed. In this instance, the amount of vanadium(III) incorporated into the lattice depended greatly on the solute to solvent ratio. Crystals with higher concentrations of vanadium(III) could be prepared by reducing the solute to solvent ratio to ca. 0.5 w/v; crystallization then occurred rapidly on cooling to room temperature. However, the amount of vanadium(III) in these α crystals was always found to be less than the amount of vanadium(III) in solution, which may result in a concentration gradient of vanadium(III) in these α crystals. Over a period of several weeks the optical quality of α crystals with high concentrations of vanadium(III) (ca. 12%) deteriorated and blue patches were noted to form on the edges of the crystals, working inward toward the center of the crystal. This is not inconsistent with an α to β phase transition, initiated in the region of the crystal where the vanadium(III) concentration is greatest followed by a cooperative α to β rearrangement. However, the microstructure of these crystals is yet to be characterised. The phase transition for a given crystal was never complete. The crystals were green in the middle and blue at the edges. Unfortunately, α crystals grown by this method were not suitable for single crystal Raman experiments, due to their poor optical quality. Doped crystals of the α modification suitable for single crystal Raman experiments were prepared by a controlled deposition method described previously (23). However, no more than ca. 7% of vanadium(III) could be incorporated into Rb[Ga:V]SH to give optically clear α crystals.

Instrumental Details

Raman spectra were obtained using a SPEX 14018 double monochrometer; the details of this instrument and sample preparation have been published previously (7, 13) Scattering experiments of the type $X'(\alpha\beta)Y'$, where X' and Y' are related to the crystallographic X and Y directions by a rotation of $\pi/4$ about Z and $\alpha\beta$ is the component of the polarizability tensor under examination, were conducted. Luminescence spectra of $CsCr(SO_4)_2 \cdot 12H_2O$ (CsCrSH) were obtained using SPEX 1401 double monochrometer equipped with 1200 groove/mm gratings a Burle C31034 GaAs photomultiplier tube and single photon counting electronics. Low-temperature measurements were made with the aid of an Oxford Instruments MD4 cryostat.

A Cary 5e spectrometer was used to collect UV/vis/NIR spectra. The polished crystals were sealed in a copper cell under a He atmosphere and cooled to ca. 16 K using a closed cycle refrigerator.

EPR spectra of RbVSH were obtained at the high-field, high-frequency EPR facility in Grenoble, France. Excitation frequencies of 94.9685, 189.937, and 284.9055 GHz were employed in conjunction with a static field ranging from 0–12 T. Spectra were recorded between 5 and 20 K. The experimental setup has been described previously (24).

3. RESULTS

Raman Spectra

The $[Rb(OH_2)_6]^+$, $[(Ga/V)(OH_2)_6]^{3+}$, and SO_4^{2-} ions all lie on sites of trigonal symmetry and the vibrations of these species will be subject to site splitting and factor group coupling (25, 26). Since the factor group coupling leads to at least one F_g component (there are three times as many F_g as A_g or E_g components) the F_g spectra are most sensitive to structural perturbations (13, 27). The F_g spectra in the region 250 and 1200 cm^{-1} are shown in Fig. 2, and this region includes the internal vibrations of the tervalent hexaaqua cation and the sulfate anion as well as the external modes of the water molecules coordinated to the mono- and tervalent cations (23, 25, 27). The F_g components of many of the modes (e.g., $\upsilon_5(M^{III}O_6)$ and $\upsilon_3(SO_4)$) are markedly different for α and β alums, as is evident from the spectra of the pure RbGaSH and RbVSH alums. The spectra permit classification of the alum type (13, 27) and confirm that the mixed alums with vanadium(III) concentrations of 25% and 45%

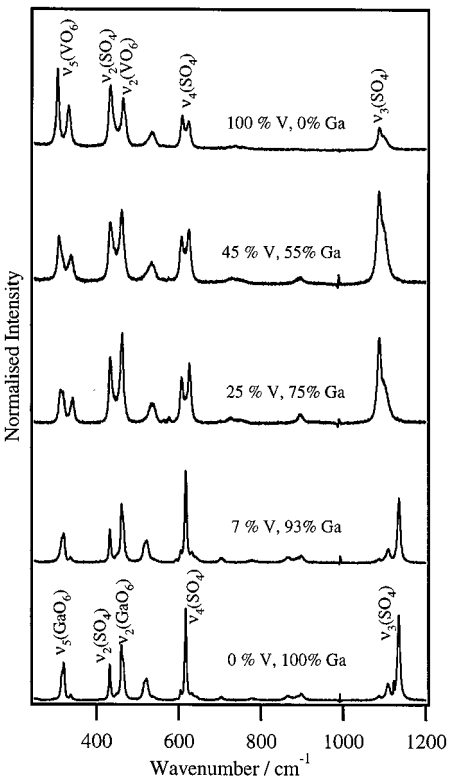

FIG. 2. Single crystal Raman spectra of Rb[Ga:V]SH, between 250 and 1200 cm^{-1}, for differing tervalent cation concentrations as indicated. Activity is $X'(ZX')Y'$: F_g. Bands of A_g and E_g symmetry, which leaked into the spectrum, were removed by spectral subtraction. All spectra obtained at ca. 80 K.

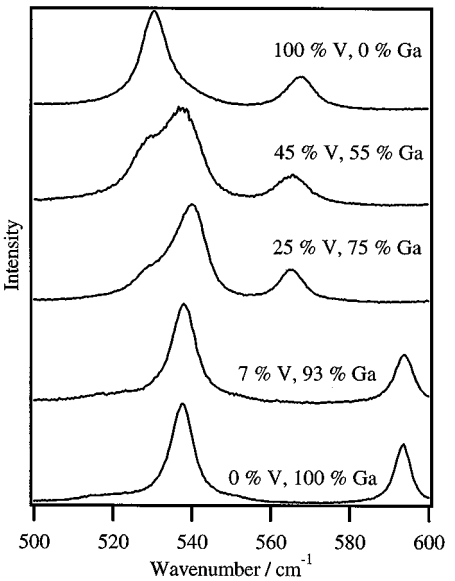

FIG. 3. Single crystal Raman spectra of Rb[Ga:V]SH, between 500 and 600 cm^{-1}, for differing tervalent cation concentrations as indicated. Activity is $X'(ZZ)Y'$: $A_g + E_g$. All spectra obtained at ca. 80 K.

crystallize as β alums whereas the mixed alum containing ca. 7% vanadium(III) adopts the α modification. The similarity of the spectra of the pure and mixed crystals suggest that the structures are well described either as α or β alums, an observation consistent with powder X-ray diffraction measurements (21). The half-widths of the bands assigned to $\upsilon_5(M^{III}O_6)$ increase and show some degree of structure on decreasing the vanadium(III) concentration from 100 to 45 and 25%. It is surprising that despite the formal lowering of the symmetry of the mixed crystals the spectra are remarkably little changed. This supports the assumption that the structures of the doped crystals may be interpreted in terms of the α and β structures of the pure alums.

The A_g and E_g spectra in the region 500–600 cm^{-1} are shown in Fig. 3. This spectral region includes A_g and E_g bands due to the external modes of water coordinated to Rb^+ ($2A_g + 2E_g$, where the A_g components are vanishingly weak) and A_g bands due to $\upsilon_1(M^{III}O_6)$ (13). Studies of the caesium alums show that $\upsilon_1(M^{III}O_6)$ is inversely proportional to $r(M^{III}\text{–O})$ (23). The V–O and Ga–O bond lengths in the rubidium alums of vanadium and gallium are 1.996 (14) and 1.952 Å (21), and the $\upsilon_1(M^{III}O_6)$ mode occurs at 530 and 538 cm^{-1}, respectively. Starting with pure RbVSH, replacement of vanadium by gallium results in a decrease in the intensity of the band due to $\upsilon_1(V^{III}O_6)$ with the concomitant growth of a new band assigned to $\upsilon_1(Ga^{III}O_6)$. This spectral region has been fitted to Lorentzian/Gaussian functions and a summary of the analysis is given in Table 1. In the mixed alums two bands of A_g symmetry are always found which correspond to the $V^{III}O_6$ and $Ga^{III}O_6$ stretches. This suggests that the A_g components of the $\upsilon_1(M^{III}O_6)$ modes are not strongly coupled and that the M^{III}–O bond lengths are characteristic of the different metals in the pure alums. Furthermore, the intensities of the bands relative to the band due to $\upsilon_1(SO_4)$ change in exact accordance with the

TABLE 1

Band Wavenumbers (cm^{-1}) and Assignments of A_g and E_g Bands between 500 and 600 cm^{-1} in the Raman Spectra of Rb[Ga:V]SH, as Shown in Fig. 3, for Different Tervalent Cation Concentrations as Indicated; ρ_5 and ρ_6 Denote External Modes of Water Coordinated to Rb^+

		0% Ga, 100% V β alum	55% Ga, 45% V β alum	75% Ga, 25% V β alum	93% Ga, 7% V α alum	100% Ga, 0% V α alum
$\upsilon_1(V^{III}O_6)$	A_g	530	529	530	531	
$\upsilon_1(Ga^{III}O_6)$	A_g		541	541	538	538
ρ_6	E_g	540	537	538	520	519
ρ_5	E_g	568	566	565	594	593

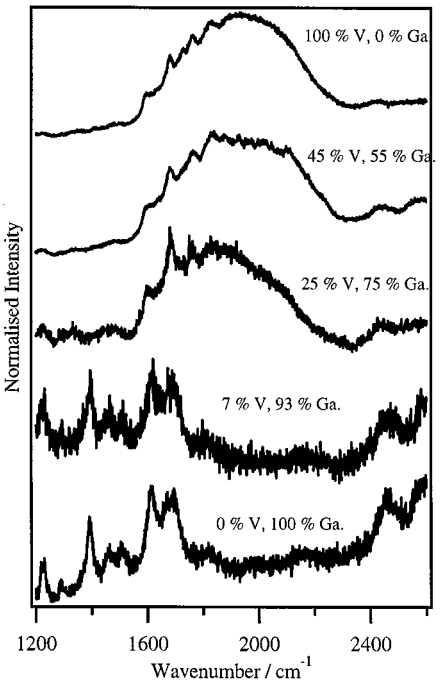

FIG. 4. Single crystal electronic Raman spectra of Rb[Ga:V]SH, between 1200 and 2600 cm^{-1}, for differing tervalent cation concentrations as indicated. Activity is $X'(ZZ)Y'$: $A_g + E_g$. All spectra obtained at ca. 80 K.

change in the relative amounts of vanadium(III) and gallium(III). The small shift in the wavenumber of $\upsilon_1(Ga^{III}O_6)$ is significant and this is likely to result from the small size mismatch between the V and Ga cations. Room-temperature powder X-ray diffraction measurements show that replacing vanadium(III) with gallium(III) leads to a decrease in the unit cell dimension and that this decrease is proportional to the gallium(III) concentration in the concentration region where the β modification is adopted.

The electronic Raman band of $[V(OH_2)_6]^{3+}$ in the β alums occurs between 1200 and 2600 cm^{-1}, and the spectra recorded in this region are shown in Fig. 4. The broad band centered at 1930 cm^{-1} has been assigned to the $^3A_g \rightarrow {}^3E_g$ (S_6) electronic Raman transition between the trigonal components of the $^3T_{1g}$ (O_h) ground term and the structure on the low-wavenumber wing to first- and second-order phonon modes not associated with the electronic transition (13, 20). The wavenumber of the electronic Raman transition is insensitive to the composition of the mixed crystal so long as the crystal adopts the β modification which implies little variation in the magnitude of the twist angle (Fig. 1). The vibrational and electronic Raman spectra suggest, therefore, that the molecular and electronic structure of $[V(OH_2)_6]^{3+}$ in mixed alums of Rb[Ga:V]SH changes little in the concentration range 25 to 100%.

For the doped α alums, Rb[Ga:V]SH, no Raman bands are found over the region 10–4000 cm^{-1} which can be assigned to an electronic Raman transition (Fig. 4); this may be due to a change in electronic structure or, alternatively, to a loss in sensitivity. The latter possibility may be excluded by examination of crystals of Cs[Ga:V]SH since these mixed alums adopt the β modification over the entire composition range. The $^3A_g \rightarrow {}^3E_g$ electronic Raman transition of vanadium(III) was apparent in the spectra of Cs[Ga:V]SH where the vanadium(III) concentration was ca. 6%. This confirms that the absence of the electronic Raman band in Rb[Ga:V]SH (7% V) is not due to the low concentration of vanadium(III) but a pronounced change in the electronic structure resulting from the change in alum modification.

Absorption Spectra

The low temperature (ca. 16 K) absorption spectra of RbVSH and Rb[Ga:V]SH (ca. 7% V) between 14,000 and 34,000 cm^{-1} are shown in Fig. 5. The spectrum of RbVSH closely resembles that of the ammonium vanadium alum[28] and is dominated by two broad bands corresponding to the $^3T_{1g}(F) \rightarrow {}^3T_{2g}(F)$ (O_h) and $^3T_{1g}(F) \rightarrow {}^3T_{1g}(P)$ (O_h) transitions. The spectrum was fitted to 4 Gaussian functions with a baseline which varied as a function of υ^4; the parameters and assignments are summarized in Table 2. The observed splittings are due to effects of the trigonal field, Jahn–Teller and spin–orbit coupling and are discussed in more detail in the next section. The electronic absorption spectrum of Rb[Ga:V]SH (ca. 7% V) also shows two broad bands each of which are shifted by ca. 1000 cm^{-1} to lower energy relative to the RbVSH spectrum, reflecting the different colors of the α and β vanadium doped crystals.

Weak absorption bands are evident in the near infrared (NIR) spectra of RbVSH (Fig. 6). These bands have a much lower intensity than those in the visible and are

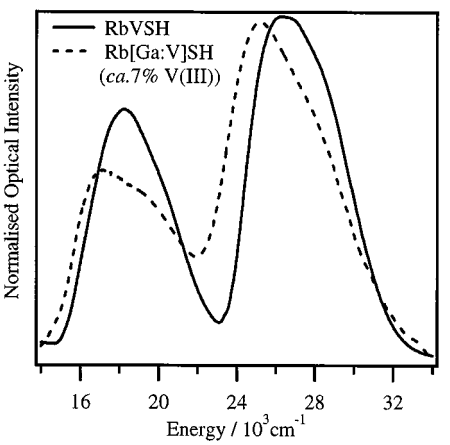

FIG. 5. Single crystal absorption spectra of RbVSH and Rb[Ga:V]SH (ca. 7% V) between 14,000 and 34,000 cm^{-1}. Both spectra obtained at ca. 16 K.

TABLE 2
Summary of the Experimental Data Obtained for RbVSH and Rb[Ga:V]SH (ca. 7% V)

Experimental technique	EPR	Electronic Raman Spectroscopy	Electronic Absorption Spectroscopy		
Experimental quantity determined	Spin-Hamiltonian parameters of ^3A_g ground term	Transition between trigonal components ($^3A_g \rightarrow {}^3E_g$) of $^3T_{1g}$ (O_h) ground term	Transition between ^3A_g and ^1E_g (S_6) ligand field terms	Transitions between $^3T_{1g}$ and $^3T_{2g}$ (O_h) ligand field terms	Transitions between $^3T_{1g}$ and $^3T_{1g}$ (O_h) ligand field terms
RbVSH	$D = 4.906(4)\ cm^{-1}$ $g_\parallel = 1.944(1)$ $g_\perp = 1.863(2)$ $A_\parallel = 111(2)$ G	$1930(10)\ cm^{-1}$	$10204(2)\ cm^{-1}$	$17{,}570(40)\ cm^{-1}$ $19{,}910(80)\ cm^{-1}$	$25{,}450(10)\ cm^{-1}$ $27{,}780(40)\ cm^{-1}$
Rb[Ga:V]SH (ca. 7% V)				$16{,}584(8)\ cm^{-1}$ $19{,}040(40)\ cm^{-1}$	$24{,}606(4)\ cm^{-1}$ $26{,}850(40)\ cm^{-1}$

a component of the $^3T_{1g} \rightarrow {}^1T_{2g}$ (O_h) transition. The NIR absorption spectrum of RbVSH is strikingly similar to the $^2E_g \rightarrow {}^4A_g$ emission of the isostructural salt CsCrSH, which has a magnetic dipole allowed origin and electric dipole allowed vibronic origins (6). By analogy, the $10{,}204(2)\ cm^{-1}$ band of RbVSH is assigned to a magnetic dipole allowed origin and the higher energy bands to vibronic origins due to ungerade vibrations of the tervalent hexaaqua cation (Table 3). The strong similarity between the two spectra shows that the vibronic intensity enabling mechanism in the alums depends on the structure of the alum and not on the identity of the mono- or tervalent cations. The assignments of the principal vibronic bands are made with reference to the single crystal Raman spectra of RbVSH (21) and CsCrSH (26) as well as recent work on the emission spectrum of Cr(III) in a variety of alums (6). The ligand field analysis suggests that the vibronic structure is built on the ^3A_g ($^3T_{1g}(O_h)$) $\rightarrow {}^1E_g$ ($^1T_{1g}(O_h)$) electronic origin. This assignment is discussed in the next section. To our knowledge this is the first time that this transition has been observed for the $[V(OH_2)_6]^{3+}$ complex.

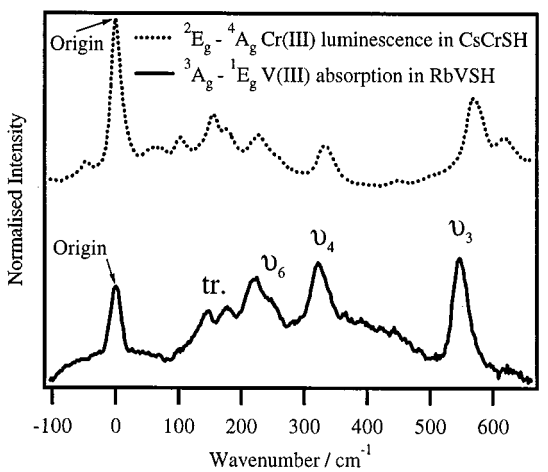

FIG. 6. Single crystal absorption spectrum of RbVSH (ca. 16 K) and single crystal luminescence spectrum of CsCrSH (ca. 80 K, 10 mW, 514.53 nm radiation at sample). The energies of the transitions have been scaled relative to the origins.

EPR Spectra

The zero field splitting (zfs) of the ^3A_g ground term of NH_4VSH ($4.95(5)\ cm^{-1}$) has been estimated from susceptibility measurements (19, 28, 29). These measurements do not permit a sufficiently precise determination of the spin-Hamiltonian parameters of the ^3A_g term to warrant a meaningful comparison with theory; for this purpose high-field, high-frequency EPR measurements have been conducted on a powdered sample of RbVSH. A total of 9 resonances were

TABLE 3
Energies (cm^{-1}) of Vibronic Bands Relative to the Electronic Origin and Assignments for the $^3A_g \rightarrow {}^1E_g$ (S_6) Absorption Spectrum of RbVSH and $^4A_g \leftarrow {}^2E_g$ Luminescence Spectrum of CsCrSH; $tr(M^{III}O_6)$ Denotes a Lattice Vibration Involving a Translation of the Tervalent Aqua Ion

	RbVSH	CsCrSH
$tr(M^{III}O_6)$	146	156
	176	173
$\upsilon_6(M^{III}O_6)$	221	227
	252	256
$\upsilon_4(M^{III}O_6)$	322	335
$\upsilon_3(M^{III}O_6)$	546	570

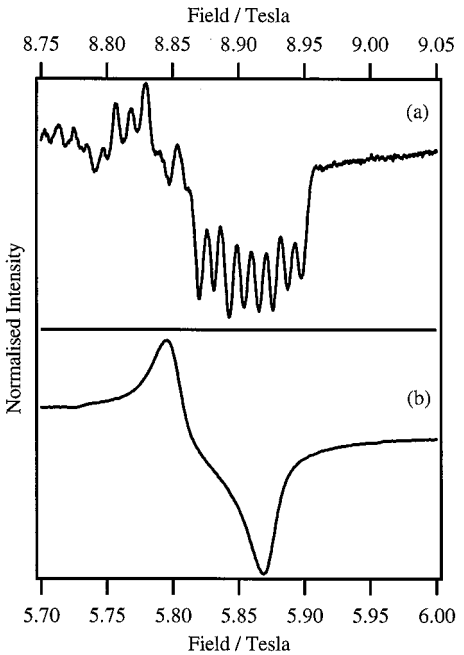

FIG. 7. Powder EPR spectra of RbVSH obtained at a frequency of 94.9685 GHz (W-band). Spectrum (a) shows an EPR resonance corresponding to the external field parallel to the S_6 axis of vanadium(III). The noise on the low-field side is due to a nonrandom distribution of the vanadium(III) ions due to incomplete grinding of the powder. An indication of the true noise level is given by the baseline on the high-field side of the transition. The EPR resonance (b) corresponds to the external field perpendicular to the S_6 axis of vanadium(III). Transitions (a) and (b) are depicted schematically in Fig. 8.

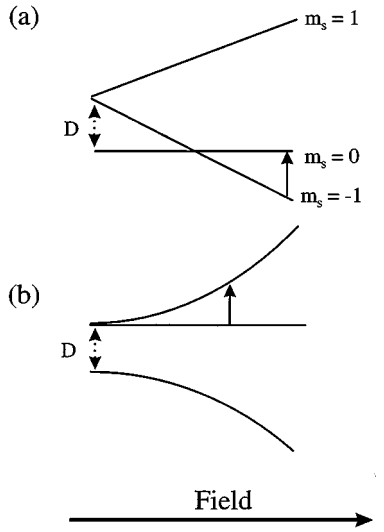

FIG. 8. Schematic energy level diagram showing EPR transitions (solid arrows) between states of the ^3A_g ground term. (a) and (b) depict the $\parallel$ and $\perp$ transitions assigned to the EPR resonances shown in Figs. 7 (a) and (b), respectively.

observed using excitation frequencies of 94.9685, 189.937, and 284.9055 GHz in conjunction with a static field ranging from 0 to 12 T. Two of the observed EPR resonances are shown in Fig. 7, and the transitions are depicted schematically in Fig. 8. The data were interpreted using the conventional spin-Hamiltonian for $(\mathbf{S, I}) = (1, \frac{7}{2})$,

$$\begin{aligned} H_s = {} & g_{zz}\,\mu_B B_z \hat{S}_z + g_{yy}\,\mu_B B_y \hat{S}_y + g_{xx}\mu_B B_x \hat{S}_x \\ & + A_{zz}\hat{S}_z\hat{I}_z + A_{yy}\hat{S}_y\hat{I}_y + A_{xx}\hat{S}_x\hat{I}_x \\ & + D[\hat{S}_Z^2 - \tfrac{1}{3}\mathrm{S}(S+1)] + E[\hat{S}_x^2 - \hat{S}_y^2], \end{aligned} \qquad [1]$$

i.e. considering the three states of the ^3A_g ground term only. At much larger magnetic fields and/or smaller trigonal field strengths, the states of the higher lying ^3E_g (S_6) term would also have to be considered in the analysis. From the recorded spectra, 8 resonances were used to determine the spin-Hamiltonian parameters. There is no suggestion of any deviation from axial anisotropy ($g_{xx} = g_{yy}$, $E = 0$) and the 8 resonances correspond to the external magnetic field being either parallel or perpendicular to the S_6 axis of vanadium(III). The parameter $A_\perp = A_{xx} = A_{yy}$ could not be determined since no resonance corresponding to the external magnetic field being perpendicular to the S_6 axis showed resolved hyperfine lines. A summary of the results and the analysis is given in Table 4. To our knowledge, this is the first time that the zfs of a d^2 complex has been determined directly by EPR spectroscopy. Under the same experimental conditions, we were unable to detect an EPR resonance for crystals of Rb[Ga:V]SH of the α type.

4. LIGAND FIELD CALCULATIONS

A summary of the experimental data obtained for RbVSH and Rb[Ga:V]SH (ca. 7%) is given in Table 2. Whereas a wealth of data has been obtained for RbVSH, for

TABLE 4
Resonant Field Positions for EPR Data Obtained for RbVSH, with Experimental Uncertainties Given in Parentheses, Estimated from the EPR Bandwidths[a]

Frequency/GHz	Observed/G	Calculated/G	Obs–calc	Assignment
94.9685	19,224 (221)	19,157	67	$\parallel$
94.9685	58,163 (181)	58,127	36	$\perp$
94.9685	88,964 (55)	88,964	0	$\parallel$
189.937	96,959 (168)	96,998	− 39	$\perp$
189.937	15,746 (55)	15,746	0	$\parallel$
189.937	23,139 (87)	23,034	105	$\perp$
189.937	34,551 (178)	34,584	− 33	$\perp$
284.9055	75,990 (200)	75,966	24	$\perp$

[a]The calculated field positions were obtained by least-squares fitting of the observed data to a $S = 1$ spin Hamiltonian (Eq. [1]). The spin Hamiltonian parameters derived from this analysis are $D = 4.906(4)\,\mathrm{cm}^{-1}$, $g_\parallel = 1.944(1)$, $g_\perp = 1.863(2)$, and $A = 111(2)$ G.

TABLE 5
Transition Energies and Ground State *g* Values Calculated Using the Angular Overlap Model (AOM)[a]

	Input for β lum	Input for α alum
Racah parameters/cm^{-1}	$B = 644$ $C = 2960$	$B = 644$ $C = 2960$
Angles for input to angular overlap model parametrization	$\theta = 55.36^\circ$ $\phi = 0^\circ$ $\psi = 66.13^\circ$	$\theta = 55.10^\circ$ $\phi = 0^\circ$ $\psi = 44.33^\circ$
Angular overlap model bonding parameters	$e_\sigma = 6950$ $e_{\pi\perp} = 930$ $e_{\pi\parallel} = 0$	$e_\sigma = 6950$ $e_{\pi\perp} = 930$ $e_{\pi\parallel} = 0$
Spin–orbit coupling constant, ζ/cm^{-1}	166.59	166.59
	Output/β	Output/α
Symmetry of trigonal ground term (S_6) and trigonal field splitting in absence of spin–orbit coupling	^3A, 1918	^3E, 1.0
Zero field splitting (cm^{-1}) and g values of ^3A ground term, $k = 1$	$D = 4.906$ $g_\parallel = 1.950$ $g_\perp = 1.847$	
Zero field splitting (cm^{-1}) and g values of ^3A ground term, $k = 0.85$	$D = 4.906$ $g_\parallel = 1.957$ $g_\perp = 1.870$	
Energies (cm^{-1}) and symmetries (S_6^*) of spin–orbit states arising from $^3T_1$ (O_h) ground term	0 Â 1826 Ê 4.906 Ê 1935 Ê 2033 Â 2043 Â	
Energies (cm^{-1}) and symmetries (S_6^*) of spin–orbit states arising from higher lying $^1T_1$ and ^1E (O_h) terms	10,207 Ê 12,108 Ê 12,378 Â	
Energies (cm^{-1}) and symmetries (S_6^*) of spin–orbit states arising from higher lying $^3T_2$ (O_h) term	18,325 Â 19,106 Â 18,330 Ê 19,107 Â 19,152 Ê 19,194 Ê	17,669 Â 17,812 Ê 17,704 Â 17,816 Â 17,719 Ê 17,782 Ê
Energies (cm^{-1}) and symmetries (S_6^*) of spin–orbit states arising from higher lying $^3T_1$ (O_h) term	26,704 Â 27,549 Â 26,709 Ê 27,562 Â 27,611 Ê 27,662 Ê	25,935 Â 26,184 Ê 25,966 Â 26,190 Â 26,003 Ê 26,092 Ê

[a]The AOM angles θ and ϕ are the usual polar angles describing the position of the oxygen atom relative to the three-fold axis; ψ is the angle between the vector normal to the plane defined by the three-fold axis and the M–O bond vector and the plane which contains the M–O bond vector and is parallel to the H–H bond vector. When the $M^{III}O_6$ framework is exactly octahedral, ψ is related to the twist angle defined in Fig. 1 by $\psi^\circ = 45^\circ - \text{twist}^\circ$. The angles for the each of the 6 coordinating water molecules may be generated by applying the symmetry operations of the S_6 point group. All terms and states are of g type and this symmetry label has therefore been omitted.

Rb[Ga:V]SH (ca. 7%) the electronic absorption spectrum is the only experimental quantity available which relates to the electronic structure of the vanadium(III) ion in the α lattice. The angular overlap model (AOM) provides a useful framework for the interpretation of optical data available for transition metal hydrates (30) and calculations were performed using the program LIGFIELD (31), written by Jesper Bendix. A summary of the ligand-field analysis is given in Table 5. For nonlinear ligators, such as water, three angles are required as input for the AOM calculations, θ, ϕ and ψ, as defined by Schäffer (30). High-quality neutron diffraction data is required to determine the value of ψ, which is not available for either RbVSH or RbGaSH. The AOM angles used in the calculation to model the RbVSH data were calculated using the fractional coordinates of $[V(OH_2)_6]^{3+}$ determined from neutron diffraction measurements on $CsV(SO_4)_2 \cdot 12D_2O$ (32). Given that RbVSH and CsVSH are isostructural and the position of the electronic Raman band in the vanadium alums does not depend on the identity of the monovalent cation, very little change in the stereochemistry of $[V(OH_2)_6]^{3+}$ is expected. The only α alum for which neutron diffraction data is available is $CsFe(SeO_4)_2 \cdot 12D_2O$ (3). The hydrogen bonds involving the water molecules coordinated to the tervalent cation are approximately linear so that the coordinates of the oxygen atoms involved in the O–H–O hydrogen bonds can be used to estimate the orientation of the water molecules. The twist, tilt and yaw angles calculated from X-ray data collected for

RbGaSH (21) are in good agreement with those calculated from the coordinates of $[Fe(OD_2)_6]^{3+}$ determined from the neutron diffraction study of $CsFe(SeO_4)_2 \cdot 12D_2O$. The fractional coordinates of the $[Fe(OD_2)_6]^{3+}$ cation in $CsFe(SeO_4)_2 \cdot 12D_2O$ were therefore used to calculate the AOM angles for the $[V(OH_2)_6]^{3+}$ cation in the α coordination geometry.

The electronic structure of $[V(OH_2)_6]^{3+}$ in the β environment may be characterized with a high degree of precision. Since the VO_6 framework is approximately octahedral, the magnitude of the e_σ parameter has little impact on the trigonal field splitting of the $^3T_{1g}$ (O_h) ground term. This is determined primarily by the magnitude and anisotropy of the e_π parameters. Polarized neutron diffraction measurements on the β-alum $CsMo(SO_4)_2 \cdot 12D_2O$ demonstrate that the π-bonding in $[Mo(OH_2)_6]^{3+}$ is significant and highly anisotropic, involving molecular orbitals normal to the plane of water molecule.[16] The sign and magnitude of the trigonal field splitting of the ground $^3T_{1g}$ (O_h) term are reproduced by setting the e_π parameter representing the π-interaction in the plane of the water molecule ($e_{\pi\|}$) to zero, and the e_π parameter, representing the π-interaction normal to the plane of the water molecule ($e_{\pi\perp}$) to ca. 930 cm^{-1}. Thus, the electronic Raman measurement fixes the magnitude of $e_{\pi\perp} - e_{\pi\|}$ and all other experimental observations must be explained with this degree of π-anisotropy as a standpoint. The energies of the $^3T_{1g}$ $(F) \rightarrow {}^3T_{2g}$ (F) (O_h) and $^3T_{1g}$ $(F) \rightarrow {}^3T_{1g}$ (P) (O_h) spin-allowed transitions are a function of e_σ, e_π, and the Racah parameter B. With $e_{\pi\perp} - e_{\pi\|}$ set to 930 cm^{-1}, the higher-lying $^3T_{2g}$ (F) (O_h) and $^3T_{1g}$ (P) (O_h) terms are each split into two components. However, the predicted splitting falls well short of that found experimentally. This result was also found by Hitchman *et al.* who used the AOM to analyze the electronic spectrum of $NH_4V(SO_4)_2 \cdot 12H_2O$ and suggested that excited state Jahn–Teller effects would act to accentuate the splittings (28). The Jahn–Teller interaction competes with the trigonal field and when the two interactions are comparable it is very difficult to establish the barry centre of the $^3T_{2g}$ (F) (O_h) and $^3T_{1g}$ (P) (O_h) terms based purely on the observation of two broad components (33). Spin-orbit coupling and vibronic coupling further complicate the interpretation of the spectrum. However, the ligand field parameters may be estimated based on the expectation that the predicted transition energies occur in an energy range which is encompassed by the two broad components found for each transition. This criteria is satisfied with the following set of parameters, $B = 644$, $e_\sigma = 6950$, $e_{\pi\perp} = 930$, $e_{\pi\|} = 0$, which are similar to the set proffered by Hitchman and co-workers for the ammonium salt (28).

The spin-forbidden transition found in the NIR is an important observation as the transition energy is strongly dependent upon the Racah parameter C. The free ion ^1D term splits into ^1T and ^1E terms in cubic symmetry, and the degeneracy is further lowered in trigonal symmetry. With $e_{\pi\perp} = 930$ and $e_{\pi\|} = 0$ the ordering of the singlet terms in increasing energy is ^1E_g ($^1T_{2g}$ (O_h)), ^1E_g (^1E_g (O_h)), and ^1A_g ($^1T_{2g}$ (O_h)). Three transitions are expected, but only one is found with vibronic structure built on an origin at 10,204(2) cm^{-1}. With B set to 644 cm^{-1}, the energy of the ^1E_g ($^1T_{2g}$ (O_h)) term is predicted to occur at 10,207 cm^{-1} with $C = 2960$ cm^{-1} giving $C/B = 4.6$. In order to assign this transition to either of the two higher lying singlet terms, C would have to be reduced substantially giving unreasonably low values of C/B, supporting assignment to the ^3A_g ($^3T_{1g}$ (O_h)) $\rightarrow {}^1E_g$ ($^1T_{2g}$ (O_h)) transition. It is likely that the other two spin-forbidden transitions, predicted around 12,108 and 12,378 cm^{-1}, are too broad to be observed. They are unlikely to be much weaker than the ^3A_g ($^3T_{1g}$ (O_h)) $\rightarrow {}^1E_g$ ($^1T_{2g}$ (O_h)) transition, because both a magnetic dipole and a vibronic electric dipole intensity mechanism provide intensity to all three transitions.

The EPR experiments determine the zfs of the ^3A_g ground term to be 4.906(4) cm^{-1}. This quantity is determined primarily by the relative magnitudes of spin–orbit coupling and the trigonal field splitting of the $^3T_{1g}$ (O_h) ground term. The quantity is less sensitive to the energies of the higher lying ligand field terms which have been estimated from the UV/vis/NIR absorption spectra. With the following ligand field parameters, $B = 644$, $C = 2960$, $e_\sigma = 6950$, $e_{\pi\perp} = 930$, and $e_{\pi\|} = 0$ cm^{-1}, the experimentally determined value of the zfs is reproduced to the precision determined from the EPR experiment with the spin-orbit coupling constant, ζ, set to 166.59 cm^{-1}, which corresponds to ca. 81% of the free-ion value (206 cm^{-1}) (34).

The final ligand field parameter to be determined is the orbital reduction factor, k, which represents the quenching of the orbital contribution to the magnetic moment and so impacts upon the ground state g values. The experimentally determined g values are $g_\| = 1.944(1)$ and $g_\perp = 1.863(2)$. Using the forementioned ligand field parameters and setting k to unity, the calculated g values are $g_\| = 1.950$ and $g_\perp = 1.847$. The value of k is expected to be less than unity on account of covalent bonding but is predicted to have a value greater than λ(complex)/λ(free ion) (35). When k is reduced to 0.85, the g values increase to $g_\| = 1.957$ and $g_\perp = 1.870$. The difference between the calculated and observed g values is well outside the precision of the measurement, for any choice of k. Setting ζ to 167 cm^{-1} and fine tuning $e_{\pi\perp}$ to reproduce D makes no difference to the calculated g values. The AOM gives a fair but not exact description of the experimental data obtained for RbVSH.

The experimental data defining the electronic structure of $[V(OH_2)_6]^{3+}$ ion in the α lattice is confined to the UV/vis absorption spectrum. However, information regarding changes to the Racah parameters which occur upon changing the mode of water coordination from the β to the α geometry can be inferred from the recent study of the Cr(III)

$^4A_g \leftarrow {}^2E_g$ emission spectrum in a variety of α and β lattices (6). It is found that the origin of this emission occurs at higher energy (ca. 450 cm^{-1}) in the α compared to the β alums, which suggests an increase in the interelectronic repulsion. This has been attributed to the tilt of the water molecules coordinated to the Cr(III) ion which is associated with the α alums (Fig. 1) (6). The $d\pi$–$p\pi$ overlap is optimal when the mode of water coordination is trigonal planar, as in the β alums, and is expected to be reduced as the water molecule is tilted away from the M–O bond vector. We have performed ligand field calculations on the Cr(III) ion in the α and β lattices and found that by keeping the ratio of C/B constant, the Racah parameters need only be increased by ca. 3% in order to reproduce the increase in the origin energy. AOM calculations for the $[V(OH_2)_6]^{3+}$ ion in the α lattice have been undertaken with two sets of parameters. In the first set, the ligand field parameters were left unchanged from the values determined from the analysis of the RbVSH data and only the AOM angles changed. In the second set, the Racah parameters were increased by ca. 3%. Similar results were obtained using the two sets of parameters and only the energies resulting from the first set are presented in Table 5. The trigonal field splitting of the $^3T_{1g}(F)$ ground term is predicted to fall practically to zero on account of the marked reduction in the twist angle (Fig. 1). Consequently, the $^3T_{1g}(F) \rightarrow {}^3T_{2g}(F)$ (O_h) and $^3T_{1g}(F) \rightarrow {}^3T_{1g}(P)$ (O_h) transitions are predicted to occur ca. 1200 cm^{-1} lower in energy in the α compared to the β lattice. This prediction is in accordance with the absorption spectra presented in Fig. 5 and is the principal reason for the pronounced color change. As well as an increase in B, an increase in ξ and a decrease in e_π might also be expected on account of the increase in the tilt angle. In addition, the energy of the ground state will be lowered as a consequence of the ground state Jahn–Teller interaction. However, insufficient data is available to quantify these effects. As for RbVSH, the $^3T_{1g}(F) \rightarrow {}^3T_{2g}(F)$ (O_h) and $^3T_{1g}(F) \rightarrow {}^3T_{1g}(P)$ (O_h) transitions in the absorption spectrum of Rb[Ga:V]SH (ca. 7% V) can each be deconvoluted into two components. The splitting of the absorption bands assigned to the $^3T_{1g}(F) \rightarrow {}^3T_{2g}(F)$ (O_h) and $^3T_{1g}(P)$ (O_h) transitions is estimated to be 2456(40) and 2244(40) cm^{-1} respectively. Since the trigonal field splitting of the $^3T_{2g}(F)$ and $^3T_{1g}(P)$ (O_h) terms is predicted to be minimal, the observed splittings are attributable to interactions such as Jahn–Teller coupling and low-symmetry strain. Clearly further experimental data, such as magnetic measurements, are required to characterize the electronic structure of vanadium(III) in the α geometry.

5. CONCLUSION

The experimental data presented for RbVSH constitute the most detailed characterization of the electronic structure of a monomeric vanadium(III) complex to date. The ligand field calculations give a fair description of the experimental data but are not able to reproduce the ground state g values determined from EPR experiments quantitatively. Preliminary work suggests that the spin-Hamiltonian parameters pertaining to the ^3A_g ground term may be strongly affected by Jahn–Teller coupling and this will be the topic of a future publication. The Raman data for mixed alums of the type Rb[Ga:V]SH show that down to concentrations of ca. one vanadium(III) ion per unit cell, the coordination geometry of $[V(OH_2)_6]^{3+}$ and the overall structure are dictated by the electronic preference of the vanadium(III) ion leading to the formation of alums of the β type. At lower vanadium(III) concentrations, the stereochemical preference of the monovalent cation dominates and the salt crystallizes in the α modification with a change in the stereochemistry of the $[V(OH_2)_6]^{3+}$ cation, imposed by hydrogen bonding constraints. This gives rise to a pronounced change in the electronic absorption spectrum. Since there is little change in $\upsilon_1(V^{III}O_6)$ associated with the $\beta \rightarrow \alpha$ structural change (and by inference that the V–O bond length is unaltered) the change in electronic structure of $[V(OH_2)_6]^{3+}$ is associated with a change in the mode of water coordination. The titanium(III) and vanadium(III) alums crystallise in the β modification, irrespective of the identity of the monovalent cation (13–15). This work strongly supports the suggestion that the failure of these alums to crystallize in the α modification is due to a marked reduction in the trigonal field stabilization energy.

ACKNOWLEDGMENTS

We thank Daniel Gamelin for useful discussions, Robin Clark for the use of his Raman spectrometer, Anne-Lavra Barra for technical assistance in obtaining the EPR spectra, and the ULIRS (University of London Intercollegiate Research Service) for the use of the 1401 double monochrometer. The Research Corporation Trust is thanked for the purchase of the MD4 cryostat. This work was funded by the Science and Engineering Research Council (studentship PLWT-P), the Australian Research Council, and the Swiss National Science Foundation.

REFERENCES

1. H. Lipson, *Phil. Mag.* **19,** 887 (1935).
   H. Lipson, *Proc. R. Soc. Lond., Ser. A* **151,** 347 (1935).
2. J. K. Beattie, S. P. Best, B. W. Skelton, and A. H. White, *J. Chem. Soc., Dalton Trans.* 2105 (1981).
3. S. P. Best and J. B. Forsyth, *J. Chem. Soc., Dalton Trans.* 395 (1990).
4. J. H. Van Vleck, *J. Chem. Phys.* **7,** 61 (1939); **7,** 72 (1939).
5. A. Manoogian and A. Leclerc, *J. Chem. Phys.* **63,** 4450 (1975).
6. R. S. Armstrong, A. J. Berry, B. D. Cole, and K. W. Nugent, *J. Chem. Soc., Dalton Trans.* 363 (1997).
7. P. L. W. Tregenna-Piggott, S. P. Best, M. C. M. O'Brien, K. S. Knight, J. B. Forsyth, and J. R. Pilbrow, *J. Am. Chem. Soc.* **119,** 3324 (1997).
8. P. L. W. Tregenna-Piggott, M. C. M. O'Brien, J. R. Pilbrow, H-U. Güdel, S. P. Best, and C. Noble, *J. Chem. Phys.* **107,** 8275 (1997).

9. P. L. W. Tregenna-Piggott, M. C. M. O'Brien, Høgni Weihe, and H.-U. Güdel, *J. Chem. Phys.* **109,** 2967 (1998).
10. S. P. Best and J. B. Forsyth, *J. Chem. Soc., Dalton Trans.* 3507 (1990).
11. S. P. Best and J. B. Forsyth, *J. Chem. Soc., Dalton Trans.* 1721 (1991).
12. S. P. Best, J. B. Forsyth, and P. L. W. Tregenna-Piggott, *J. Chem. Soc., Dalton Trans.* 2711 (1993).
13. P. L. W. Tregenna-Piggott and S. P. Best, *Inorg. Chem.* **35,** 5730 (1996).
14. J. K. Beattie, S. P. Best, P. Del Favero, B. W. Skelton, A. N. Sobolev, and A. H. White, *J. Chem. Soc., Dalton Trans.* 1481 (1996).
15. S. Haussühl, *Z. Kristallogr., Kristallgeom. Kristallphys., Kristallchem.* **116,** 371, (1961).
16. S. P. Best, B. N. Figgis, J. B. Forsyth, P. A. Reynolds, and P. L. W. Tregenna-Piggott, *Inorg. Chem.* **34,** 4605 (1995).
17. C. Daul and A. Goursot, *Inorg. Chem.* **24,** 3554 (1985).
18. H. Tachikawa, T. Ichikawa, and H. Yoshida, *J. Am. Chem. Soc.* **112,** 982 (1990).
19. B. N. Figgis, J. Lewis, and F. E. Mabbs, *J. Chem. Soc.* 2480 (1960).
20. S. P. Best and R. J. H. Clark, *Chem. Phys. Lett.* **122,** 401 (1985).
21. P. L. W. Tregenna-Piggott and S. P. Best, unpublished work.
22. S. P. Best, R. S. Armstrong, and J. K. Beattie, *Inorg. Chem.* **19,** 1958 (1980).
23. S. P. Best, J. K. Beattie, and R. S. Armstrong, *J. Chem. Soc., Dalton Trans.* 2611 (1984).
24. (a) F. Muller, A. Hopkins, N. Coron, M. Grynberg, L. C. Brunel, and G. Martinez, *Rev. Sci. Instrum.* **60,** 3681 (1989). (b) A. L. Barra, L. C. Brunel, and J. B. Robert, *Chem. Phys. Lett.* **165,** 107 (1990).
25. S. P. Best, R. S. Armstrong, and J. K. Beattie, *J. Chem. Soc., Dalton 2Trans.*, 1655 (1982).
26. J. K. Beattie, R. S. Armstrong, and S. P. Best, *Spectrochim. Acta* **51A,** 539 (1996).
27. R. S. Armstrong, J. K. Beattie, S. P. Best, B. W. Skelton, and A. H. White, *J. Chem. Soc., Dalton Trans.* 1973 (1983).
28. M.A. Hitchman, R. G. McDonald, P. W. Smith, and R. Stranger, *J. Chem. Soc., Dalton Trans.* 1393 (1988).
29. (a) J. Van der Handel and A. Siegert, *Physica* **4,** 871 (1937). (b) J. J. Fritz and H. L. Pinch, *J. Am. Chem. Soc.* **78,** 6223 (1956).
30. C.E. Schäffer, *Structure Bonding* **5,** 68 (1968).
31. J. Bendix, "LIGFIELD: An Extensive Program Package for Ligand Field Calculations on a Personal Computer," *in* Proceedings of the 29th ICCC, Lausanne, Switzerland, 1992.
32. S. P. Best, P. L. W. Tregenna-Piggott, and C. C. Wilson, unpublished work.
33. (a) M. C. M. O'Brien, "Vibronic Spectra and Structure Assoicated with Jahn–Teller Interactions in the Solid State," *in* Vibrational Spectral and Structure (J. R. Durig, Ed.), pp. 321–394. Elsevier, Amsterdam, 1981. (b) I. B. Bersuker, "The Jahn–Teller Effect and Vibronic Interactions in Modern Chemistry." Plenum Press, New York, 1984.
34. J. Bendix, M. Brorson, and C. E. Scäffer, *Inorg. Chem.* **32,** 2838 (1993).
35. A. Abragam, and B. Bleaney, "Electron Paramagnetic Resonance of Transition Metal Ions." Oxford Univ. Press, Oxford, 1970.